Science of the Total Environment 663 (2019) 369–379

Contents lists available at ScienceDirect

Science of the Total Environment

journal homepage: www.elsevier.com/locate/scitotenv

Interaction between carbon dioxide emissions and eutrophication in a drinking water reservoir: A three-dimensional ecological modeling approach

Zhonghan Chen, Ping Huang *, Zhou Zhang

Department of Environmental Science, School of Environmental Science and Engineering, Sun Yat-sen University, Guangzhou 510275, China

HIGHLIGHTS

- The ecological model was developed to simulate CO_2 emission from a reservoir.
- The surface CO_2 concentration showed no significant difference between seasons.
- The surface CO_2 concentrations were high in inflow and dam regions.
- The interactions among CO_2 emission, eutrophication and climate change
- The analysis of carbon cycle showed 32% carbon retention efficiency.

GRAPHICAL ABSTRACT

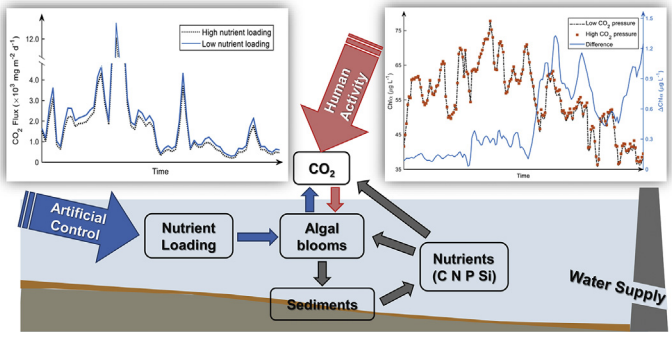

ARTICLE INFO

Article history:
Received 10 November 2018
Received in revised form 24 January 2019
Accepted 25 January 2019
Available online 29 January 2019

Editor: Ashantha Goonetilleke

Keywords:
Greenhouse gases emission
Numerical modeling
Phytoplankton
Reservoirs
Climate change
Carbon cycle

ABSTRACT

We developed a three-dimensional model to study the dynamics of carbon dioxide (CO_2) emission from a subtropical drinking water reservoir. The quantitative effects of dissolved CO_2 concentration on phytoplankton growth were coupled in an inorganic carbon module. Water quality monitoring was carried out to calibrate and validate the model. The simulated surface CO_2 concentrations showed no significant difference between seasons ($p > 0.05$). Regarding the spatial distribution, high CO_2 concentrations were observed in the inflow and dam regions ($p < 0.05$). Four scenarios of different atmospheric CO_2 pressures and eutrophic levels were simulated to test the following hypotheses: (1) eutrophication will reverse the carbon budgets in reservoir systems and (2) rising CO_2 levels will increase phytoplankton biomass. The results showed that water quality improvements will promote the emission of CO_2 into the atmosphere. Simultaneously, the elevated CO_2 in the air will stimulate algal biomass, especially in nutrient-rich systems. The systematic analysis of carbon cycling revealed the different internal transformation rates under different scenarios and showed that 32% of carbon was removed via CO_2 emission and carbon burial. The interaction provides a novel direction to understand the feedback loops between aquatic ecosystems and increasing CO_2 pressure in the future.

1. Introduction

During the recent two decades, the studies on greenhouse gases (GHGs) emission from reservoirs, especially those in boreal and Amazon regions, have confirmed the role of reservoirs as GHG sources

* Corresponding author.
E-mail addresses: chenzhh43@mail2.sysu.edu.cn (Z. Chen), eeshping@mail.sysu.edu.cn (P. Huang), zhangzh35@mail2.sysu.edu.cn (Z. Zhang).

https://doi.org/10.1016/j.scitotenv.2019.01.336
0048-9697/

(Barros et al., 2011). Among the common types of GHGs, the fluxes of carbon dioxide (CO_2) are the most widely available because diffusion is the dominant flux pathway across the air-water interface (Deemer et al., 2016). Based on measurements in previous studies, various statistical analyses were performed to estimate the global CO_2 emission (Chen et al., 2018; Barros et al., 2011; St. Louis et al., 2000). However, nearly 80% of the data used for global estimations were derived from studies on hydroelectric systems, while the area of reservoirs used for energy generation represents only 25% of the area of all reservoirs in the word (Song et al., 2018). Although the statistical analysis showed that there was no significant difference between CO_2 emission from hydroelectric and nonhydroelectric reservoirs, the different dam operational regimes and retention time might affect CO_2 emission pattern (Deemer et al., 2016; Pacheco et al., 2015). Prior reports indicated that the inflow areas generally displayed elevated CO_2 emission and the areas close to the dam were generally characterized by low concentrations in hydropower reservoirs (Pacheco et al., 2015; Paranaíba et al., 2018). The typical pattern of CO_2 emission in other types of reservoirs was not reported (Deemer et al., 2016). Therefore, more measurements and studies are needed in other types of systems to adequately understand the carbon emission patterns and reliably estimate global emissions.

The fluxes of CO_2 are likely to be controlled by many potential factors that vary among different reservoirs. At global or regional scales, the temperature and initial organic carbon in the flooded area were considered as the key factors in CO_2 dynamics (Barros et al., 2011). For particular types of reservoirs, a study on 39 drinking water reservoirs in Germany indicated that high CO_2 emission often occurred in reservoirs with low pH and total alkalinity (Saidi and Koschorreck, 2017). In addition to the large-scale diversity, the spatiotemporal heterogeneity of CO_2 emission in reservoirs has been documented in many studies (Morales-Pineda et al., 2014; Teodoru et al., 2011). This variability is commonly attributed to the dynamics of metabolic activity and meteorological conditions (Morales-Pineda et al., 2014) and episodically related to water-level fluctuations or thermal stratification of the water column (Pacheco et al., 2015; Tonetta et al., 2017). Consequently, understanding the different forcing factors is essential for an accurate estimation of the carbon cycle as well as effective control of the efflux of CO_2.

In contrast to the recent interest in reservoirs as CO_2 sources, there have been long-term efforts to control eutrophication risks. Recently, the potential relationship between eutrophication and CO_2 emission has attracted much attention under climate change conditions. A vicious feedback loop was proposed, wherein a warming climate with high atmospheric CO_2 concentration supports large algal populations and primary production; then, the produced CO_2 diffuses to the atmosphere, leading to further climate warming and increased CO_2 pressure (Deemer et al., 2016). The analysis of 69 boreal lakes with different CO_2 gradients showed that elevated CO_2 concentration promoted phytoplankton biomass and was unlikely to influence the composition (Vogt et al., 2017). In this comparative study among lakes, neither the absolute biomass nor the relative biomass of algal groups varied predictably along with the CO_2 gradients. In contrast, in situ microcosm experiments in a subtropical lake, which can predict the variety of phytoplankton by manipulating CO_2 concentrations, showed that increased CO_2 could affect the phytoplankton community structure but not change the productivity (Shi et al., 2017). These small scale experiments were designed by not considering the interactive effects from CO_2 in combination with other variables, such as hydrodynamic conditions and limited nutrients. Furthermore, laboratory experiments were designed to identify the effect of elevated CO_2 on phytoplankton, and these experiments indicated that the differences between major taxonomic groups in both genetic diversity and physiological flexibility could lead to species-specific responses (Low-Décarie et al., 2014). Consequently, it is promising and necessary to synthetically study the feedback mechanisms among CO_2 emission, eutrophication and climate change.

Given the complexities mentioned above, numerical models have shown high application potential for the study of CO_2 emission and carbon dynamics. Statistical models, such as GHG risk assessment tool (GRAT), were developed on the basis of existing CO_2 measurements and applied to estimate regional or global emissions (Kumar and Sharma, 2016; Kumar et al., 2018; Kumar et al., 2019). Unlike statistical models, process-based models can describe the boundless carbon cycle along terrestrial–aquatic continuum by integrating a set of equations. However, these coupled models on a large scale were likely to ignore the metabolism (Tian et al., 2015) or simplify the reservoirs to well-mixed steady flows (Nakayama and Pelletier, 2018). To describe the transport of carbon from sediment to atmosphere through water column in details, one-dimensional biogeochemistry models were developed to predict the CO_2 emission from young reservoirs, such as the Forest Aquatic-Denitrification Decomposition (FAQ-DNDC) model (Wang et al., 2018). Moreover, three-dimensional hydrodynamic and ecological models can further simulate the spatial-temporal dynamics of carbon under complex flow conditions. Curtarelli et al. (2016) applied the Estuary and Lake and Coastal Ocean Model-Computation Aquatic Ecosystem Dynamics Model (ELCOM-CAEDYM) to simulate CO_2 emission from an Amazon hydroelectric reservoir, which was validated by the observed CO_2 data, and accurately estimated the annual flux. However, these ecological models are not specific enough to understand the relationship between phytoplankton growth and CO_2 concentrations. Only simplified phytoplankton growth models with CO_2 and one or two other limiting factors have been built to explore the response of phytoplankton to rising CO_2 availability (Ji et al., 2017; Verspagen et al., 2014). Therefore, incorporating the detailed feedback between phytoplankton growth and CO_2 into large-scale ecological models of reservoirs can help researchers to confidently predict the responses of aquatic biota to climate change.

In this study, a three-dimensional hydroelectric and water quality model was adapted to simulate surface CO_2 emission and eutrophication in a drinking water reservoir in a subtropical zone. The results of the hydrodynamic and ecological modules are calibrated and validated by comparing the simulated variables with field observations. With the help of this model, we can study the spatial and temporal variations in CO_2 concentration and the potential environmental drivers because the model was developed by coupling a module to describe the effects of inorganic carbon on phytoplankton growth. In this way, we can further explore two questions through setting scenarios: 1) how the elevated atmospheric CO_2 pressure in the future will impact algal growth and biomass, and 2) whether reservoirs with low trophic levels tend to emit more CO_2 than those with high trophic levels.

2. Materials and methods

2.1. Study site and sampling

The drinking water reservoir evaluated in this study is located in southeast China and has a subtropical maritime climate with a mean annual temperature of 22.4 ± 0.6 °C (mean ± standard deviation (SD)) and a mean annual precipitation of 1933.0 ± 414.9 mm. Because of the legal requirements for water supply security, this reservoir will remain anonymous and is referred to as the SY reservoir in this study (Fig. 1(a)). The SY reservoir was built in the 1960s for flood prevention and agricultural irrigation and first converted to a drinking water storage and supply reservoir in 2000. The SY reservoir is a medium-sized reservoir with a total storage capacity of 32 million m^3 and an average depth of 4.6 m, which guarantees a daily average drinking water supply of 0.9 million m^3. As the last reservoir in a cascade reservoir group, the main water flowing into the SY reservoir is from the upstream reservoir via a water diversion tunnel.

The eight sampling sites were distributed in the mainstream of the reservoir from the inflow area to the dam (Fig. 1(a)). At each sampling site, we measured the water temperature (T_{water}, °C), salinity (Sal, PSU),

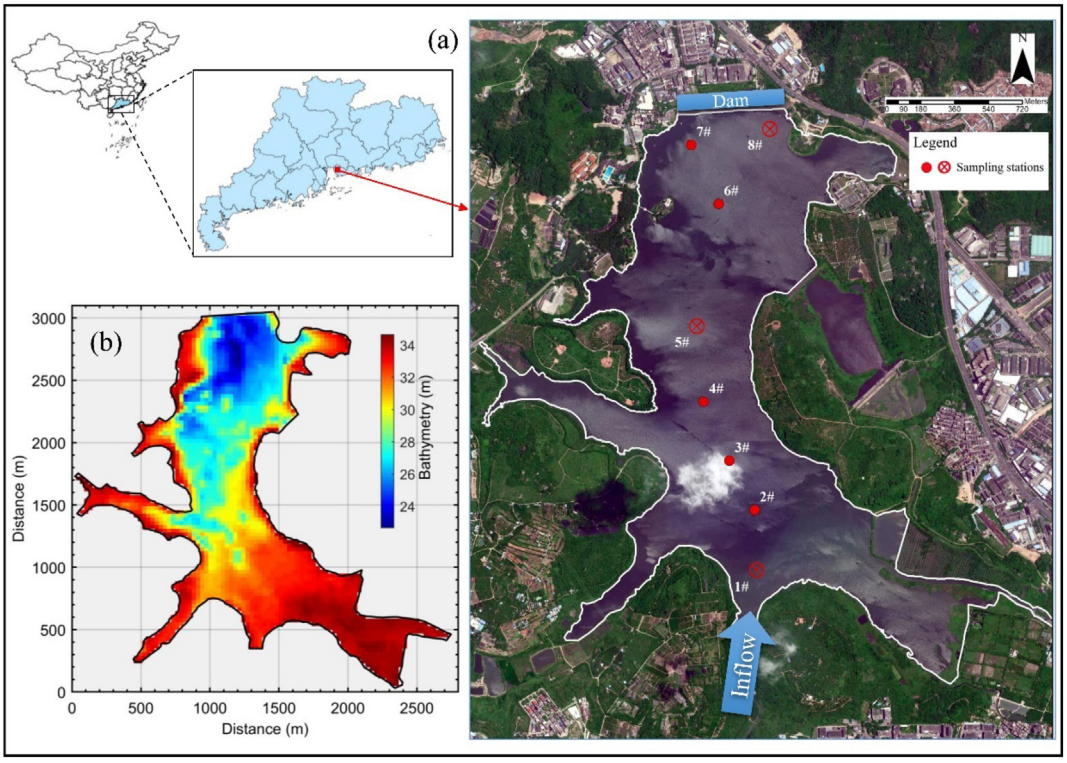

Fig. 1. Study area: (a) satellite image of the studied reservoir and the sampling sites; (b) boundary and bathymetry used for the simulations.

pH, dissolved oxygen (DO, mg L^{-1}) and chlorophyll α (Chlα, μg L^{-1}) in the surface, euphotic and bottom layers (if necessary, the thermocline layer was also measured) using a multiparameter water quality data sensors (YSI-6600V2). A standard 30 cm diameter Secchi disk was used to measure the Secchi disk depth (SDD, m). The other water quality variables included total alkalinity (TA, meq L^{-1}), ammonium (NH_4-N, mg L^{-1}), nitrate (NO_3-N, mg L^{-1}), total nitrogen (TN, mg L^{-1}), phosphate (PO_4-P, mg L^{-1}), total phosphorus (TP, mg L^{-1}), dissolved silicate (SiO_4-Si, mg L^{-1}) and total organic carbon (TOC, mg L^{-1}), which were measured in the laboratory following standard national methods (APHA, 2005). Water samples from the first, fifth and eighth sites were also collected for phytoplankton analysis. Phytoplankton samples fixed with Lugol's solution were identified and enumerated under a trinocular optical microscope (OLYMPUS MX60) to determine the phytoplankton biomass. The digital camera was used to transfer the photomicrographs to computer, and the cell sizes of dominant species were directly measured using the software offered by Olympus Company. Field monitoring was conducted at approximately 15-day intervals, while the laboratory measurements were carried out monthly in the period from 30 May to 1 December 2013. The statistical parameters for measured variables and the correlation results are shown in Tables S1 and S2, respectively.

2.2. 3D hydro-ecological model description

Delft3D is an open-source 2D/3D software package for the analysis of hydrodynamics, sediment transport, morphology and water quality for fluvial, estuarine and coastal environments (https://oss.deltares.nl/web/delft3d). In this study, the FLOW and WAQ modules in Delft3D (version 4.03.01) were used as the modeling tools. This framework has been successfully applied to simulate circulation patterns, thermal stratification, water quality, and climate impacts in various aquatic systems (Han et al., 2016; Li and Reidenbach, 2014). The main reason for the selection of Delft3D was that the WAQ module considers CO_2 balance (Menshutkin et al., 2014).

2.2.1. Hydrodynamic Delft3D-FLOW model

The hydrodynamic model (Delft3D-FLOW) solves the Navier-Stokes equations for an incompressible fluid under shallow water assumptions using the finite difference method (Deltares, 2017b). This model calculates the transport of heat as a function of advective and dispersive fluxes in three coordinate directions.

An orthogonal curvilinear grid was developed using the Delft3D-Refgrid grid generator, resulting in a total of 2800 computational grid cells with a typical resolution of 30 m × 30 m. The bathymetry data (Fig. 1(b)) were provided by the local municipal water affairs bureau and linearly interpolated onto the grid network using QUICKIN (Deltares, 2017c). The vertical grid discretization was defined as 6 uniformly distributed sigma layers. The model was run for the period from 1 June 2013 to 30 November 2013. The time step of the simulation was 1 min, and the simulated data were output every 15 min.

The meteorological data for the simulations included daily atmospheric pressure (P_{atm}, h Pa), air temperature (T_{air}, °C), solar radiation (SR, W m^{-2}), relative humidity (RH, %), cloud cover (C, %), wind speed (W_{speed}, m s^{-1}), wind direction ($W_{direction}$, °), evaporation (EV, mm d^{-1}) and precipitation (P, mm d^{-1}) data, which were provided from the meteorological stations near the SY reservoir via the China Meteorological Data Sharing Service System (http://cdc.cma.gov.cn/home.do). The monthly precipitation during simulation period is shown in Fig. S1. The daily water level and exchange flow data were provided by the local municipal water affairs bureau.

Among the different turbulence closure schemes, the k-epsilon model was selected because of its sufficient accuracy in the case of stratification. The Ocean Heat Flux Model was applied for heat transfer across the water surface based on the specified net SR. The bottom roughness was prescribed with a constant bed roughness length (Z_0).

The wind shear stress was considered and could also be determined by a quadratic expression. The reservoir was considered closed, and the water balance was maintained by regulating the inflow and outflow. This condition ensures convenient adjustments of the vertical positions of intakes and outfalls. During the simulating period, the SY reservoir discharged bottom water to increase vertical mixing and dissipation of bottom materials.

2.2.2. Ecological Delft3D-WAQ model

The Delft3D-WAQ module aims to solve the advection-diffusion-reaction equation on a computational grid in conjunction with the FLOW module. This ecological module provides a framework for a wide range of user-selected substances and processes with improved flexibility to simulate physical, (bio)chemical and biological processes (Deltares, 2017a; Deltares, 2017d). Given the objectives of this study, the phytoplankton dynamics, nutrient cycling and inorganic carbon balance were considered as the key processes in both the water column and sediment layer and the interactions between the bottom and overlying water. The structure of the water quality model designed in this study is schematized briefly in Fig. S2.

To simulate the phytoplankton dynamics, ECO in the Delft3D-WAQ module was applied to model the species competition and adaptation to temperature, limiting nutrients and light. Based on the measured phytoplankton community composition in the SY reservoir, three phytoplankton groups were selected: green algae, freshwater diatoms and blue-green algae. The different phenotypes of a species group were modeled as separate variables with different parameters for the maximum rates of primary production, respiration, mortality and sedimentation. The actual biomass stoichiometry depends on the relevant environmental factors, including temperature, nutrients and light. Furthermore, inorganic carbon was also considered a rate-limiting resource for phytoplankton, which was measured as a function of CO_2 and bicarbonate (HCO_3) availability for photosynthesis (Lim_C) (Verspagen et al., 2014):

$$Lim_C = \frac{\frac{u_{MAX,CO2} \times [CO_2]}{H_{CO2} + [CO_2]} + \frac{u_{MAX,HCO3} \times [HCO_3]}{H_{HCO3} + [HCO_3]}}{u_{MAX,CO2} + u_{MAX,HCO3}}$$

where $u_{MAX,CO2}$ and $u_{MAX,HCO3}$ are the maximum uptake rates of CO_2 and HCO_3, respectively, and H_{CO2} and H_{HCO3} are their half-saturation constants. The values of Lim_C are in the range of 0 to 1. If CO_2 and HCO_3 are both freely available, Lim_C will be close to 1. These parameters are difficult to calibrate because they are species-specific. As a result, the dominant species in the SY reservoir and previous estimations from monoculture experiments were both considered for the determination of parameters, which are shown in Table 1.

Nutrient cycles include the transitions among algae, inorganic components and organic matter. The state variables in the algae process were carbon, nitrogen, phosphorus and silicate in cells. The inorganic components mainly included NH_4-N, NO_3-N, PO_4-P, SiO_4-Si and total inorganic carbon (TIC, mg L^{-1}). The organic matter was described as the mineralization and conversion of the particulate fraction and the mineralization of the dissolved fraction. The interactions in water column, in sediment layer and between bottom and overlying water were simulated with a simplified sediment model. The upper fraction of sediment (0.1 m) was considered the active layer, which acted as a nutrient source and an oxygen sink to the overlying water.

Table 1
Parameter values for the carbon limitation function.

Algae	Dominant species	$u_{MAX,CO2}$ μmol L^{-1} d^{-1}	H_{CO2} μmol L^{-1} d^{-1}	$u_{MAX,HCO3}$ μmol L^{-1} d^{-1}	H_{CO3} μmol L^{-1} d^{-1}
Greens	*Chlorella* sp.	22.5[a]	2.5[a]	15.7[a]	40.0[a]
Diatoms	*Melosira* sp.	28.2[b]	1.7[b]	20.1[b]	12.0[b]
Blue-green	*Microcystis* sp.	20.1[c]	1.0[c]	10.8[c]	20.0[c]

[a] The value is presented in Ji et al. (2017).
[b] The value is presented in Burkhardt et al. (2001).
[c] The value is presented in Ji et al. (2017).

The main processes of inorganic carbon balance are atmospheric exchange of CO_2, mineralization of organic carbon to inorganic carbon, respiration of zooplankton and algal primary production. TIC is defined as the sum of CO_2, HCO_3 and carbonate (CO_3), which is essentially in equilibrium with TA and pH. The TA reflects the acid-neutralizing capacity of water and changes with the assimilation of nitrate and phosphate. Based on TIC and TA, the pH and relative proportions of TIC species can be calculated. The reaeration of CO_2 was calculated according to the Wanninkhof equation (Wanninkhof, 2014), in which the saturation concentration was formulated as a function of temperature and salinity (Weiss, 1974). Compared to the frequently used the Wanninkhof equation (Wanninkhof, 1992), the updated equation (Wanninkhof, 2014) can calculate gas exchange in an extended temperature range. The quantity of reaeration per day was equivalent to the flux of CO_2 (FCO_2, mg C m^{-2} d^{-1}) that diffused across the air-water interface. In this study, positive values of FCO_2 indicated that the reservoir acted as a carbon source, while negative values indicated that the reservoir acted as a sink of carbon to the atmosphere.

The ecological model was simulated with the same grid as the hydrodynamic model. Mass transport between segments was derived from Delft3D-FLOW on a quarter-hourly basis and one output per day was generated. The daily concentrations of substances, including Sal, DO, Chlα, pH, TA, NH_4-N, NO_3-N, PO_4-P andSiO_4-Si, from the upstream reservoir were extrapolated by linear interpolation of monthly field measurements. Some parameters were assessed indirectly for the water quality simulation, including the contents of organic carbon, organic nitrogen, organic phosphorus in water and in algae cells (in the Supplementary document). The parameter values for phytoplankton in the eutrophication module are shown in Table S3.

2.3. Model validation and evaluation

The parameters of the hydrodynamic and ecological models were calibrated by using a trial-and-error method based on field measurements in June, July and August 2013. The data for the remaining months (September to November) were used for model validation. We calibrated and validated the hydrodynamic module using water level and water temperature data. For the water level, we compared the simulated results with daily monitoring at the dam provided by the local municipal water affairs bureau. Moreover, the water level observations, which were derived from the field measurements of water depth and altitude of each sample site, were also used for comparison. The measured indices of DO, Chlα, NH_4-N, NO_3-N, TN, PO_4-P, TP, SiO_4-Si, TOC and SDD were selected to calibrate and validate the water quality module. In addition, the surface water concentrations of CO_2 were calculated from the observed T_{water}, Sal, pH and TA of the surface water by semiempirical equations for calibration and validation. The semiempirical equations have been developed as the 'seacarb' package in R (Lavigne et al., 2014), which has been applied in many freshwater reservoirs to calculate CO_2 emission (Saidi and Koschorreck, 2017; Wen et al., 2017). Even though some previous studies noted an overestimation of TA and pH measurement caused by the failure to account for noncarbonate alkalinity (Hunt et al., 2011), this measurement still remained useful to describe the aquatic chemistry. In addition, the noncarbonate alkalinity has a low magnitude in the SY reservoir because of the high pH (pH > 7.4). Therefore, the uncertainty of the estimation by the 'seacarb' package could be minimized.

To quantitatively evaluate the model performance, three performance metrics were selected: root mean square difference (RMSD), relative root mean square error (RRE) and Nash-Sutcliffe efficiency (NSE). Smaller RMSD and RRE values and larger NSE values indicate better model performance. Typically, RRE values < 30% and NSE values > 0

are considered acceptable. In addition to numerical metrics, the techniques of target and Taylor diagrams were also used to compactly display the model performance (in the Supplementary document).

2.4. Statistical analysis

To test whether the group distributions are different, the Kruskal Wallis nonparametric analysis is suitable when the data do not have a normal distribution with homogenous variances. Kruskal Wallis test is based on an analysis of mean ranks with the null hypothesis that the data are from populations with the same location. To identify the strength of the correlation between variables, the Spearman's rank correlation coefficient is often used for data with no exact distribution through comparing the similarity of rankings. In this study, the statistical analysis and figures were made using MATLAB R2017b.

2.5. Scenarios setup

With the help of the validated model, simulations under different scenarios are valuable for evaluating the relationships among atmospheric CO_2 pressure, eutrophication and carbon emissions. In consideration of the trends of increasing atmospheric concentration and eutrophication control, the scenarios were set by improving the CO_2 pressure in the air and reducing the nutrient load. The actual conditions acted as a reference scenario (RE scenario), while three scenarios were defined by modifying the conditions, as shown in Table 2.

The Intergovernmental Panel on Climate Change (IPCC) predicted that the concentration of CO_2 in the atmosphere is likely to triple by 2100 (IPCC, 2014). In this study, we set atmospheric CO_2 pressure to 538 ppm (RCP4.5) to describe the potential future climate condition (CL scenario). Meanwhile, the nutrient loads were regulated to study the CO_2 emission at different eutrophic levels. The ratio between TN and TP in the SY reservoir was approximately 93.3 ± 30.7, which is much larger than the canonical Redfield ratio of 16. In this phosphorus-limited water, the inflow loading of only TP would be decreased by 25% of the base scenario to control eutrophication (EU scenario). Furthermore, an integrated scenario was established to understand the combined effects (C&E scenario).

3. Results

3.1. Calibration and validation results

The hydrodynamic module was calibrated and validated for water level and water temperature by comparing the model outputs to the observations. The simulated water levels strongly corresponded to the observed values in different samples as well as the daily water level measured at the dam (Fig. S3). The model showed a slight tendency to underestimate the water level, which can be explained by the neglect of the tributary during the simulations. The water in the tributary is intercepted by the runoff control systems before it flows into the SY reservoir; therefore, the contribution from the tributary was considered minor. The performance metrics for the hydrodynamic and ecological models are presented in Table S4 for both the calibration and validation data sets, which show that the performance of the model is acceptable.

Target-Taylor diagrams generated using pointwise comparisons at each sampling time are shown in Fig. 2(a1, a2), which indicates that

Table 2
Model scenarios are the combination of two atmospheric CO_2 pressures ($CO2_{atom}$) and two modes of TP concentration in inflow loading (TP_{inflow}).

ID	Scenarios			
	RE	CL	EU	C&E
$CO2_{atom}$	316 ppm	538 ppm	316 ppm	538 ppm
TP_{inflow}	100%	100%	75%	75%

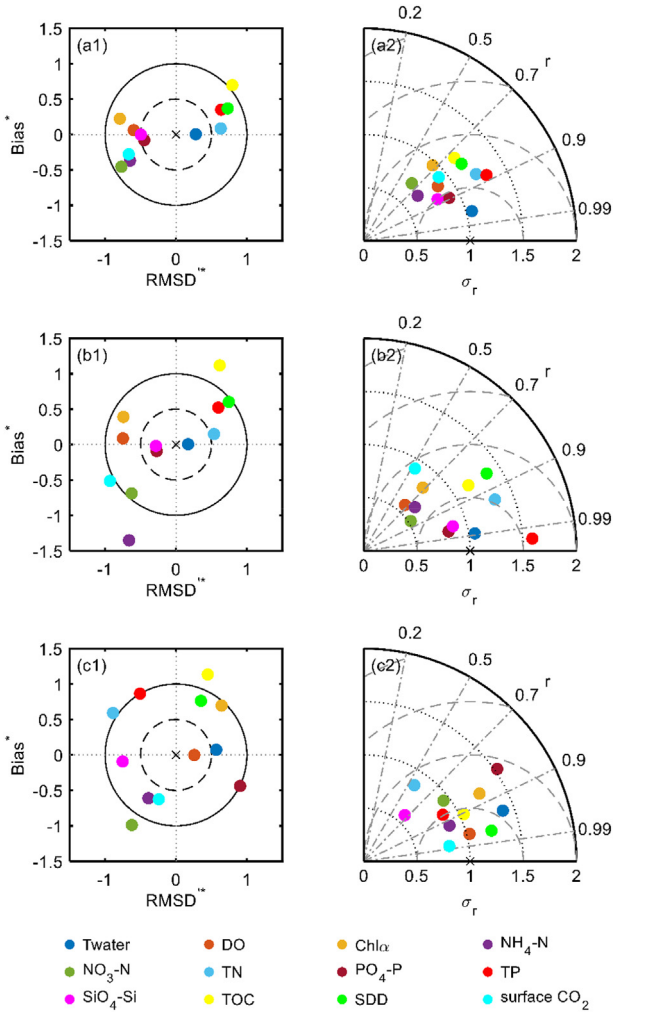

Fig. 2. Target (left panel) and Taylor (right panel) diagrams illustrating the model skills for the hydrodynamic and biogeochemical fields. Circles in (a1) and (a2) represent model skill, which was calculated by pointwise comparisons; circles in (b1) and (b2) represent temporal model skill, which was calculated by comparing the time series of spatial mean observational and model data; circles in (c1) and (c2) represent spatial model skill, which was calculated by comparing the spatial series of the temporal mean observational and model data. The crosses represent reference points. $RMSD'^*$ represents the normalized unbiased root-mean-squared difference; $Bias^*$ represents the normalized bias; r represents the correlation coefficient; σ_r represents the ratio between the SD of the simulations and observations. On the target diagram, the distance from the reference point is proportional to the total RMSD. On the Taylor diagram, the distance between model points and the reference point are proportional to the unbiased RMSD.

model skill statistics are acceptable ($r > 0.64$, absolute $RMSD'^* < 0.79$, absolute $Bias^* < 0.69$). In both diagrams, TOC points appear farthest from the reference points due to a poor correlation as well as an overestimate of the values, resulting in the large RRE (23.63%) and low NSE (−0.11). The temperature points appear closest at a low RRE (7.40%) and high NSE (0.92). The other diagrams in Fig. 2(b1, b2) and (c1, c2) show the temporal and spatial model skills, respectively. The simulated distributions exhibit a good phase agreement with the observed values ($r > 0.52$) at both the temporal and spatial scales. The high RMSD of NH_4-N in the time series might be associated with the neglect of precipitation and the inflow of the small tributary. In contrast, the high spatial error of SiO_4-Si and PO_4-P resulted from the high σ_r, which can be attributed to the simplified sediment module. For the surface CO_2 concentrations, the correlation is higher for the spatial series ($r = 0.98$) than for the temporal series ($r = 0.53$), and the SDs of the simulations are similar to the estimations by the 'seacarb' package ($0.81 < \sigma_r < 0.92$). The observed CO_2 data, which were derived from TA and pH measurements, are thought to be slightly overestimated (Hunt et al., 2011). The

negative Bias* of surface CO_2 might be explained by this overestimation. As another key variable in this study, the simulated Chlα concentrations tended to be somewhat higher than the observations (Bias* > 0); the coefficient that attained by pointwise comparisons is approximately 0.68, whereas the temporal correlation is as high as 0.86.

3.2. Surface water CO_2 concentrations and environmental drivers

The concentration of CO_2 at the surface from the inflow to the dam region along the sample sites from a daily time series is shown in Fig. 3(a). The line charts of the spatial mean and temporal mean values are plotted in Fig. 3(b) and (c), respectively. During the summer period, the surface-averaged CO_2 ranged from 0.19 mg L^{-1} to 1.92 mg L^{-1}, with a mean value of 0.78 mg L^{-1} and a SD of 0.41 mg L^{-1}. During the autumn period, the surface-averaged CO_2 ranged from 0.28 mg L^{-1} to 1.36 mg L^{-1} with a mean value of 0.74 mg L^{-1} and SD of 0.21 mg L^{-1}. Because the data of surface CO_2 did not fit a normal distribution (Kolmogorov-Smirnov test, $p < 0.001$), Kruskal Wallis test was selected to analyze the differences. The results showed no significant differences between summer and autumn ($\chi^2 = 0$, $p = 0.98$ $\chi^2 = 0$, $p = 0.98$). Besides, both the riverine (0.79 ± 0.02 mg L^{-1}) and dam zones (0.77 ± 0.01 mg L^{-1}) had higher CO_2 concentrations than the main body of the SY reservoir (0.73 ± 0.03 mg L^{-1}). Based on the temporal mean data at three different parts of the reservoir, the significant differences were observed among regions (Kruskal Wallis test, $\chi^2 = 27.55$, $p < 0.05$). The results of further multiple comparison tests showed the difference between the inflow zone and dam zone was not significant ($p = 0.63$), while the CO_2 concentrations in the main body were significantly differed from both the inflow and dam zones ($p < 0.05$).

Spearman correlation analysis was conducted to explore the potential factors that may impact the concentration and distribution of surface CO_2 and FCO_2. Spearman correlation analysis was selected because the data of CO_2 and FCO_2 were not normally distributed (Kolmogorov-Smirnov test, $p < 0.001$), even after logarithmic transformation. The main meteorological factors were selected, including daily P_{atm}, T_{air}, SR, RH, W_{speed} and P. The influence of hydrodynamic processes was assessed by Schmidt's Stability index (ST, J/m^2), which is defined as the energy required to transform the present density distribution into a new uniformity (Idso, 1973). The ST value is zero when the water column is isothermal and maximum when a water body is most strongly stratified (Winder and Schindler, 2004). The environmental variables for correlation analysis were T_{water}, DO, Chlα, TN, TP, TOC at the surface and SDD. These values were used as a time series derived from the results of the simulations. The results of the correlation analysis are shown in Table S5. Not surprisingly, a significant relationship existed between CO_2 concentration and FCO_2 ($r = 0.837$), which indicated that a reservoir with high CO_2 tends to emit more CO_2. The high negative correlation coefficients with surface CO_2 were observed for the following variables: DO, Chlα, TP and TOC. Only the W_{speed} and SDD showed significant positive correlations with the CO_2 concentrations. On the other hand, more meteorological variables showed high correlations with FCO_2, such as P_{atm}, T_{air} and RH.

3.3. Climate and nutrient scenarios

Four scenarios (Table 2) were simulated by the validated model. The spatially averaged FCO_2 values during the simulated period under various scenarios are shown in Fig. 4. Compared to RE scenario, the SY reservoir emits less CO_2 (−135.11% ± 106.02%) under future climate conditions with high atmospheric CO_2 pressure (CL scenario). In contrast, there would be more CO_2 (32.78% ± 25.32%) emission from this reservoir with decreased nutrition loadings (EU scenario). Under the combined effect of improved atmospheric CO_2 and controlled P loadings (C&E scenario), the flux of CO_2 ranged between the fluxes under the EU to CL scenarios, and the emission patterns were similar to those under the CL scenario, especially in autumn.

To explore the impact of elevated CO_2 pressure on water quality, the differences in Chlα (ΔChlα) were calculated between the Chlα values simulated under different scenarios (Fig. 5). At both nutrient levels, elevated CO_2 pressure tended to increase algal biomass (0.78% ± 0.72%) while exhibiting temporal and spatial variations. The effects on Chlα were more pronounced during autumn (1.22% ± 0.69%) than summer (0.23% ± 0.17%). The effects on Chlα at the lower TP level (0.70% ± 0.69%) increased less than that under the high TP level (0.85% ± 0.74%). The concentrations of Chlα increased more in the surface layers than in the deep layers than in the surface layers in autumn, while the pattern was reversed in summer.

Furthermore, ΔChlα on 27 August and 21 November are shown in detail in Fig. 6. These dates were selected because the measured concentrations of Chlα on 27 August and 21 November were the highest and lowest among the 10 sampling times, respectively. The phytoplankton can be strongly stimulated in the shallow water parts of the SY reservoir, which are the algal bloom-prone zones. The comparisons between scenarios could lead to the conclusion that increased CO_2 could promote

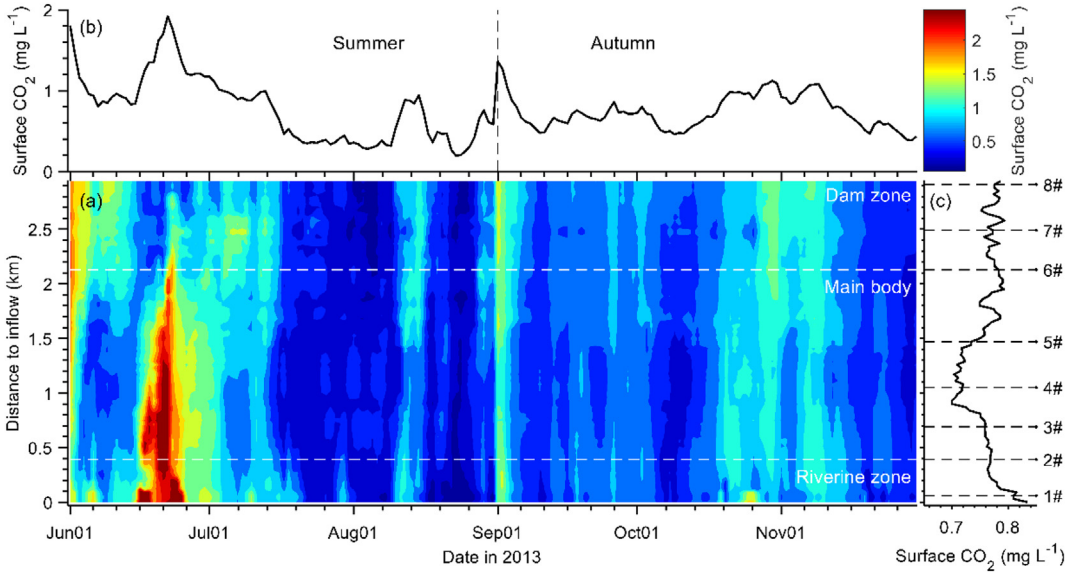

Fig. 3. Temporal and spatial variations in surface CO_2 concentrations. (a) Surface CO_2 concentrations from the inflow to the dam region along the sample sites during spring and autumn in 2013; (b) time series of longitudinal mean CO_2 concentrations at the surface; and (c) longitudinal series of temporal mean CO_2 concentrations at the surface.

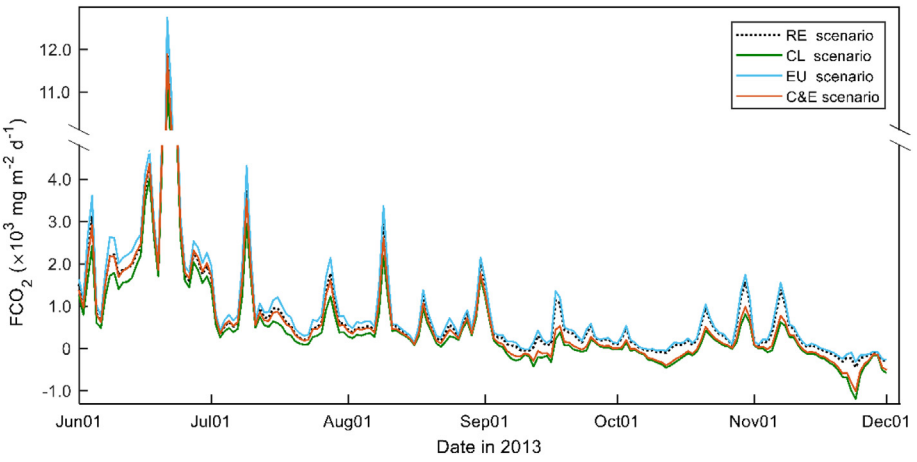

Fig. 4. Time series of the simulated flux of CO_2 (FCO_2) under four scenarios. The dotted line represents FCO_2 under the RE scenario with real atmospheric CO_2 pressure (316 ppm) and real phosphorus loading. The green line represents FCO_2 under the CL scenario with high atmospheric CO_2 pressure (538 ppm) and real total phosphorus loading. The blue line represents FCO_2 of the EU scenario with real atmospheric CO_2 pressure (316 ppm) and decreased total phosphorus loading (75%). The orange line represents FCO_2 of the C&E scenario with high atmospheric CO_2 pressure (538 ppm) and decreased total phosphorus loading (75%). (For interpretation of the references to color in this figure legend, the reader is referred to the web version of this article.)

algal biomass more actively at high eutrophic levels than at low eutrophic levels.

3.4. Systematic carbon transformations

The production and consumption rates of inorganic carbon (IC) and organic carbon (OC) in the system under different scenarios are presented in Fig. 7. In addition to inflow and outflow, the main processes of carbon cycling included the net primary production of phytoplankton, the respiration of zooplankton, the mineralization in both sediment and water column, the burial of OC and the reaeration of CO_2 at the water-atmosphere interface. The transformation rates were estimated from the mass results, which were computed as an output file from the model simulation. The output values are the sum of the process transformation rates over the model simulation period. Thus each process rate would be divided by the simulated days to get a daily mean value.

The C retention was defined as the permanent removal of C from aquatic system. The C retention rate was calculated from the sum of the transport rates of reaeration and burial processes, which should equal to the difference between C inputs and C outputs. Within the SY reservoir, C retention efficiencies (retention rate/input rate) under different scenarios could be calculated for comparison. This approach was common in the nitrogen (N) retention studies (Han et al., 2016; Harrison et al., 2009). The high atmospheric CO_2 pressure (CL scenario) would limit CO_2 emission and improve the primary production, thus converting more IC into OC (105 mg m^{-3} d^{-1}) and decreasing C retention efficiency in this reservoir (19%). At low trophic level (EU scenario), the rates of primary production and mineralization would decrease, accompanying with the low conversion rate of IC (85 mg m^{-3} d^{-1}) and the high C retention efficiency (35%).

4. Discussion

4.1. Temporal and spatial variations in CO_2 emission

In this study, there was no significant difference of the surface CO_2 concentrations between seasons in the SY reservoir. Previous studies through both field monitoring and modeling indicated the variable patterns of gas fluxes, which were attributed to the complex meteorological, hydrodynamic and ecological factors (Curtarelli et al., 2016; Pacheco et al., 2015; Roland et al., 2010). Based on the results of the correlation

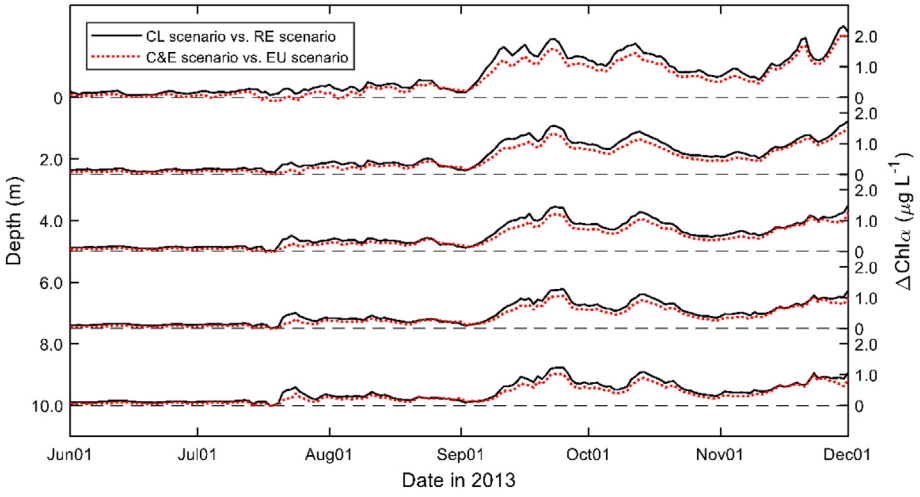

Fig. 5. Comparison of the difference in Chlα (ΔChlα) at five depths (0, 2.5, 5, 7.5 and 10 m). The solid black line represents ΔChlα between the CL scenario and the RE scenario, which shows the effect of CO_2 on Chlα at a high nutrient level. The dotted red line represents ΔChlα between the C&E scenario and EU scenario, which shows the effect of CO_2 on Chlα at a relatively low nutrient level. (For interpretation of the references to color in this figure legend, the reader is referred to the web version of this article.)

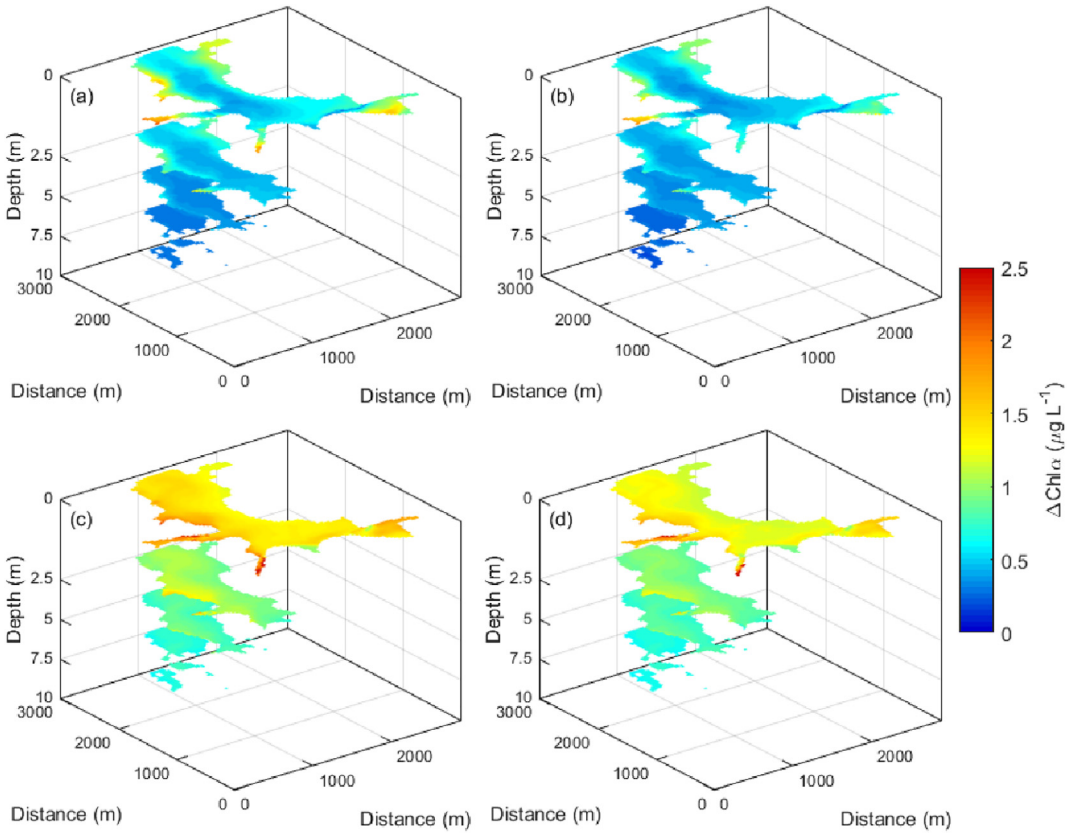

Fig. 6. 3D modeled Chlα difference (ΔChlα) under four scenarios at five depths (0, 2.5, 5, 7.5 and 10 m). (a) ΔChlα between the CL scenario and RE scenario at midday on 27 August 2013; (b) ΔChlα between the C&E scenario and EU scenario at midday on 27 August 2013; (c) ΔChlα between the CL scenario and RE scenario at midday on 21 November 2013; and (d) ΔChlα between the C&E scenario and EU scenario at midday on 21 November 2013.

analysis in this study, CO_2 tended to be enriched in the surface water, especially when the reservoir was in a low trophic state. Santoso et al. (2017) measured the diffusive CO_2 emission across lakes with various trophic states and found that improved water quality was associated with both increased surface water CO_2 concentrations and CO_2 emission to the atmosphere. Meanwhile, the results of regression analysis based on the measurements of 16 small dams in China also showed that eutrophication conditions could act as a good predictor of CO_2 concentrations

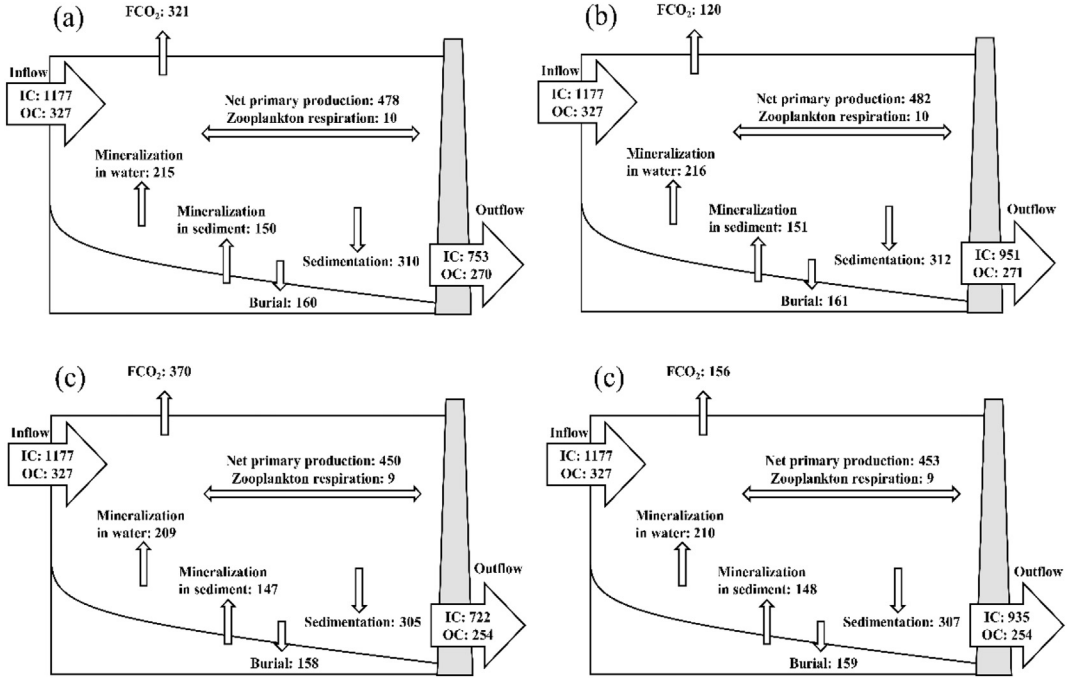

Fig. 7. Overview of the systematic carbon transformation rates (mg C m^{-3} d^{-1}) in the SY reservoir under four scenarios during the simulation period. (a) RE scenario; (b) CL scenario; (c) EU scenario; and (d) C&E scenario.

(Wang et al., 2017). In addition, the significant correlation of meteorological factors may indicate that climatic conditions dominated the CO_2 emission. This result is coincident with the results of previous studies showing that gases might escape more easily from surface water when the air pressure is low (Xiao et al., 2013). In this model, the gas transfer velocity was calculated as a function of wind speed and water column stability (Wanninkhof, 2014), resulting in the conclusion from the correlation analysis that CO_2 can escape more easily at higher wind speeds. Some studies have also suggested a positive link between CO_2 emission and wind speed (Duchemin et al., 1999); however, gas exchange seems to be less relevant in some low-wind lakes (Crusius and Wanninkhof, 2003). Therefore, the gas transfer function needs to be further optimized and validated under different wind speeds.

The CO_2 concentrations in the surface water in the inflow and outflow regions were higher than those in other regions. These spatial patterns are generally associated with the hydrodynamic conditions in old reservoirs. Furthermore, as the last reservoir in a cascade of reservoirs, the SY reservoir might receive CO_2-rich hypolimnetic waters from the upstream reservoir. A previous study showed that the downstream reservoir in a cascade reservoir-river system maintained a high CO_2 concentration (Wang et al., 2011). Because physical obstacles can result in the discontinuity of water chemistry, integrated models of cascade reservoir-river systems are needed to explore the complex carbon dynamics.

In previous studies, global CO_2 emission was estimated based on data collected near the dam. Roland et al. (2010) sampled five reservoirs and showed that ignoring the spatial variability might lead to an underestimation of >25% of the total system diffusive flux because the dam areas showed low CO_2 saturation, which was similar to the observations (Pacheco et al., 2015; Paranaíba et al., 2018). However, the simulations in the SY reservoir indicated that the concentrations of CO_2 were relatively high in both the inflow and dam regions. This discrepancy might be associated with the types of reservoirs and operation styles. Accordingly, we consider that lacustrine-style reservoirs for water supply have strong disturbances and perturbations in dam areas, resulting in high gas emissions. More researches on the patterns of the spatial variation in different types of reservoir ecosystems are clearly needed.

4.2. Feedbacks between eutrophication and atmospheric CO_2 pressure

The simulations under different scenarios demonstrated that the decreases in trophic state were associated with increased CO_2 emission to the atmosphere. This result is in line with the results of studies on temperate lakes suggesting that lakes undergoing eutrophication can become atmospheric CO_2 sinks (Knoll et al., 2013; Pacheco et al., 2014). The aquatic ecosystems with high phytoplankton productivity generally consume a large amount of CO_2 for photosynthesis. Simultaneously, abundant CO_2 could be produced through organic matter decomposition, which would be accumulated in the water column and sediment because of algal blooms (Yan et al., 2017). Therefore, the net balance between these two processes can determine whether eutrophication would reverse the carbon budgets (Almeida et al., 2016). In the SY reservoir, controlling TP load would reduce the net primary production rate more significantly than the mineralization rate, thus emitting more CO_2. This effect might be more detectable in summer due to the high efficiency of biochemical reactions under higher temperature. On the other hand, the elevated atmospheric CO_2 pressure can certainly induce the influx of carbon into water, especially in autumn when the saturation concentration of CO_2 is high. Therefore, under this potential climatic condition combined with the artificial control of eutrophication, the carbon dynamics would achieve a new balance between influx and efflux of CO_2.

As a key nutrient for algal productivity, CO_2 is always neglected during the control of eutrophication in freshwater systems because of its high global availability. However, increased primary production and biomass of phytoplankton have been observed as the result of elevated atmospheric CO_2 (Low-Décarie et al., 2014). CO_2 is likely to be a rate-limiting resource, whereas phosphorus is a yield-limiting resource (Low-Décarie et al., 2014). The concentration of rate-limiting resources would affect the speed of biomass accretion, whereas the total amount of yield-limiting resources would limit the potential maximum of biomass present in a system. Therefore, the threshold concentrations below which algae are no longer able to withdraw this nutrient from the ambient water were set for the dominant nutrients (N, P and Si) but not for inorganic carbon, so as to distinguish between different limiting-types of resources. Moreover, CO_2 and other nutrients such as phosphorus have a synergistic effect on phytoplankton (Jansson et al., 2012; Low-Décarie et al., 2014). In this model, the carbon limitation was described by a multiplier (Lim_C) on the growth rate to simulate the colimitation involving other nutrients.

Our results likely reflect that elevated CO_2 could stimulate algal growth under TP-rich conditions. Jansson et al. (2012) performed experimental manipulation of the CO_2 concentration in supersaturated boreal lakes and found that the phytoplankton biomass could be controlled by the colimitation of CO_2 and phosphorus. This stimulation can be explained by the fact that the activity of enzymes for carbon-concentration mechanisms (CCMs) might increase with phosphorus enrichment (Beardall et al., 2005; Reinfelder, 2010; Wu et al., 2012).

The more considerable impact of high atmospheric CO_2 levels on phytoplankton in autumn can be attributed in part to the diversity of the community composition. The results of both measurements and simulations in the SY reservoir showed that cyanobacteria were the primary species, especially during summer, while green algae and diatoms were more dominant in autumn. In this model, three taxonomic groups were assigned specific parameters for $Lim_C Lim_C$. The Lim_C values for blue-green algae were highest at the same CO_2 level, while those for green algae exhibited the sharpest increased with the increase in inorganic carbon concentration. This result was in line with the results of in situ experiments and empirical laboratory studies that indicated that cyanobacteria are thought to be superior competitors at low dissolved CO_2 concentrations, whereas eukaryotic phytoplankton, such as green algae, may benefit more from elevated CO_2 (Low-Décarie et al., 2011; Shi et al., 2017). However, some recent studies have presented the opposite views because such simple dichotomies cannot combine the diversity of CCMs within and among taxa (Sandrini et al., 2016; Sandrini et al., 2014). Therefore, further refinement of the underlying physiological and ecological processes is necessary to improve the model predictions.

The responses of phytoplankton population densities to rising CO_2 are predicted to vary over space. However, few realistic whole-system experiments have explored this spatial variation (Shapiro, 1997). Theoretically, the algae in surface water are more sensitive to the change of atmospheric CO_2, because of the direct gas transfer at the air-water interface and the available light for photosynthesis. If other nutrients were sufficient or the eukaryotic phytoplankton were dominant in the surface water, the algal biomass was likely to increase significantly. In autumn, the concentrations of TN, TP, SiO_4-Si and the proportion of greens and diatoms were higher, which might explain why Chlα increased more in the surface layers than in the deep layers. However, algal biomass in the deep layer was increased more during summer. One explanation is that the concentrations of TP, which can promote the response of algae to CO_2, were much higher in the deep layer. TP might be accumulated by precipitation in the water column and resuspension from sediments. Moreover, cyanobacteria, which are the primary species in summer, can seek to exploit nutrients in deep waters. The response of phytoplankton to rising CO_2 levels was stronger in the littoral zone than in the main water body. Verspagen et al. (2014) considered that primary production in shallow water appeared to be more sensitive to atmospheric CO_2 elevation than that in deep water.

4.3. Comparison with previous studies and future research directions

During the simulation period, the daily FCO_2 at each grid point was extracted from the models. As a result, the SY reservoir is a CO_2 source

with a flux of 320.78 ± 486.39 mg C m^{-2} d^{-1}. The CO_2 emission from the SY reservoir was higher than that from natural lakes (648 mg C m^{-2} d^{-1}), but lower than the reservoirs (288 mg C m^{-2} d^{-1}) of Chinese eastern plain region, on which the SY reservoir was located (Wen et al., 2017). This might be attributed to the age of the SY reservoir (60 years old). Previous studies showed a clear decrease trend in FCO_2 with the reservoir age (Barros et al., 2011; Curtarelli et al., 2016). As a mesotrophic reservoir (Carlson's trophic index) in the subtropical region, the estimated OC burial rate in the SY reservoir (160.30 ± 31.53 mg C m^{-2} d^{-1}) was lower than the value in the tropical eutrophic reservoir (440 mg C m^{-2} d^{-1}) and higher than the values in the oligotrophic systems (116 mg C m^{-2} d^{-1}) (Table S6). Indeed, OC burial rates of eutrophic deep systems are commonly higher at high latitude regions (Almeida et al., 2016). Besides, previous studies showed that the carbon retention efficiencies in lakes and reservoirs ranged from 20% to 75% of the carbon input (Tranvik et al., 2009). Comparing the SY reservoir with other reservoirs, the carbon retention efficiency was moderately low (32%).

Uncertainty of the hydrodynamic and water quality models might be caused by a variety of routes, such as natural stochasticity, uncertainty of model structure and parameter uncertainty (Pei and Wang, 2003). There were some potential sources of error and uncertain in this study. First, the simulated CO_2 concentrations were verified by the derived data from semiempirical equations. Second, the atmospheric deposition of materials onto reservoir surfaces was not considered and the zooplankton communities were simplified as only one species in the model. Third, the parameters in the Wanninkhof equation, which was used to calculate CO_2 exchange in the model, have an uncertainty of 20% (Wanninkhof, 2014).

In this study, the SY reservoir is the last one of a cascade reservoir group; thus, the hydrodynamics and loads are relative simple. In the future, the hydrodynamic and ecological models can be used to simulate other types of reservoirs for comparison. Furthermore, the model could also be coupled with watershed models and climate-carbon cycle models to predict the responses to future climate and help design effective environmental policies for managing aquatic ecosystems.

5. Conclusions

Numerical models are potential tools to explore the complex interactions within ecosystems. In this study, a three-dimensional ecological model was developed to simulate algal blooms and carbon dynamics in a drinking water reservoir, which attracts less attention than hydropower reservoirs in terms of studies on CO_2 emission. The spatial variations in surface CO_2 were obvious, while there was no significant difference between seasons. During the simulation period, approximately 32% of total carbon was removed from the system via CO_2 emission and OC burial in the SY reservoir. Furthermore, the validated model was applied under different atmospheric CO_2 pressures and TP levels to test several hypotheses. High nutrient concentrations could increase the effect of CO_2 pressure on eutrophication; therefore, controlling nutrient loading not only resolves current water quality problems but also reduces possible eutrophication risks under climate change. However, under the scenario with low TP loading, the reservoir might emit more CO_2, which provides positive feedback to climate change. In the future, coupled climatic and aquatic models have the potential to fully and accurately describe this feedback loop.

Appendix A. Supplementary data

Supplementary data to this article can be found online at https://doi.org/10.1016/j.scitotenv.2019.01.336.

References

Almeida, R.M., Nobrega, G.N., Junger, P.C., et al., 2016. High primary production contrasts with intense carbon emission in a eutrophic tropical reservoir. Front. Microbiol. 7, 717. https://doi.org/10.3389/fmicb.2016.00717.

APHA, 2005. Standard Methods for the Examination of Water and Wastewater. 21st ed. American Public Health Association, Washington, DC, New York.

Barros, N., Cole, J.J., Tranvik, L.J., et al., 2011. Carbon emission from hydroelectric reservoirs linked to reservoir age and latitude. Nat. Geosci. 4, 593–596. https://doi.org/10.1038/ngeo1211.

Beardall, J., Roberts, S., Raven, J.A., 2005. Regulation of inorganic carbon acquisition by phosphorus limitation in the green alga Chlorella emersonii. Can. J. Bot. 83, 859–864. https://doi.org/10.1139/B05-070.

Burkhardt, S., Amoroso, G., Riebesell, U., et al., 2001. CO_2 and HCO_3-uptake in marine diatoms acclimated to different CO_2 concentrations. Limnol. Oceanogr. 46, 1378–1391. https://doi.org/10.4319/lo.2001.46.6.1378.

Chen, Z., Ye, X., Huang, P., 2018. Estimating carbon dioxide (CO_2) emissions from reservoirs using artificial neural networks. Water 10, 26. https://doi.org/10.3390/w10010026.

Crusius, J., Wanninkhof, R., 2003. Gas transfer velocities measured at low wind speed over a lake. Limnol. Oceanogr. 48, 1010–1017. https://doi.org/10.4319/lo.2003.48.3.1010.

Curtarelli, M.P., Ogashawara, I., de Araújo, C.A.S., et al., 2016. Carbon dioxide emissions from Tucuruí reservoir (Amazon biome): new findings based on three-dimensional ecological model simulations. Sci. Total Environ. 551–552, 676–694. https://doi.org/10.1016/j.scitotenv.2016.02.001.

Deemer, B.R., Harrison, J.A., Li, S., et al., 2016. Greenhouse gas emissions from reservoir water surfaces: a new global synthesis. Bioscience 66, 949–964. https://doi.org/10.1093/biosci/biw117.

Deltares, 2017a. D-water Quality Processes Library Description: Technical Reference Manual. Deltares, The Netherlands.

Deltares, 2017b. Hydro-moephdynamics: User Manual. Deltares, the Netherlands.

Deltares, 2017c. QUICKIN: User Manual. Deltares, The Netherlands.

Deltares, 2017d. Water Quality and Aquatic Ecology: User Manual. Deltares, The Netherlands.

Duchemin, E., Lucotte, M., Canuel, R., 1999. Comparison of static chamber and thin boundary layer equation methods for measuring greenhouse gas emissions from large water bodies. Environ. Sci. Technol. 33, 350–357. https://doi.org/10.1021/es9800840.

Han, H.J., Los, F.J., Burger, D.F., et al., 2016. A modelling approach to determine systematic nitrogen transformations in a tropical reservoir. Ecol. Eng. 94, 37–49. https://doi.org/10.1016/j.ecoleng.2016.05.054.

Harrison, J.A., Maranger, R.J., Alexander, R.B., et al., 2009. The regional and global significance of nitrogen removal in lakes and reservoirs. Biogeochemistry 93, 143–157. https://doi.org/10.1007/s10533-008-9272-x.

Hunt, C.W., Salisbury, J.E., Vandemark, D., 2011. Contribution of non-carbonate anions to total alkalinity and overestimation of pCO_2 in New England and New Brunswick rivers. Biogeosciences 8, 3069–3076. https://doi.org/10.5194/bg-8-3069-2011.

Idso, S.B., 1973. On the concept of lake stability. Limnol. Oceanogr. 18, 681–683. https://doi.org/10.4319/lo.1973.18.4.0681.

IPCC, 2014. Climate Change 2014: Impacts, Adaptation, and Vulnerability. Part A: Global and Sectoral Aspects. Contribution of Working Group II to the Fifth Assessment Report of the Intergovernmental Panel on Climate Change. Cambridge University Press, Cambridge, United Kingdom and New York, NY, USA.

Jansson, M., Karlsson, J., Jonsson, A., 2012. Carbon dioxide supersaturation promotes primary production in lakes. Ecol. Lett. 15, 527–532. https://doi.org/10.1111/j.1461-0248.2012.01762.x.

Ji, X., Verspagen, J.M.H., Stomp, M., et al., 2017. Competition between cyanobacteria and green algae at low versus elevated CO_2: who will win, and why? J. Exp. Bot. 68, 3815–3828. https://doi.org/10.1093/jxb/erx027.

Knoll, L.B., Vanni, M.J., Renwick, W.H., et al., 2013. Temperate reservoirs are large carbon sinks and small CO_2 sources: results from high-resolution carbon budgets. Glob. Biogeochem. Cycles 27, 52–64. https://doi.org/10.1002/gbc.20020.

Kumar, A., Sharma, M.P., 2016. Assessment of risk of GHG emissions from Tehri hydropower reservoir, India. Hum. Ecol. Risk Assess. Int. J. 22, 71–85. https://doi.org/10.1080/10807039.2015.1055708.

Kumar, A., Sharma, M.P., Yang, T., 2018. Estimation of carbon stock for greenhouse gas emissions from hydropower reservoirs. Stoch. Env. Res. Risk A. 32, 3183–3193. https://doi.org/10.1007/s00477-018-1608-z.

Kumar, A., Yang, T., Sharma, M.P., 2019. Long-term prediction of greenhouse gas risk to the Chinese hydropower reservoirs. Sci. Total Environ. 646, 300–308. https://doi.org/10.1016/j.scitotenv.2018.07.314.

Lavigne, H., Epitalon, J.M., Gattuso, J.M., 2014. seacarb: Seawater Carbonate Chemistry With R. R package. R Package Version.

Li, A.G., Reidenbach, M.A., 2014. Forecasting decadal changes in sea surface temperatures and coral bleaching within a Caribbean coral reef. Coral Reefs 33, 847–861. https://doi.org/10.1007/s00338-014-1162-1.

Low-Décarie, E., Fussmann, G.F., Bell, G., 2011. The effect of elevated CO_2 on growth and competition in experimental phytoplankton communities. Glob. Chang. Biol. 17, 2525–2535. https://doi.org/10.1111/j.1365-2486.2011.02402.x.

Low-Décarie, E., Fussmann, G.F., Bell, G., 2014. Aquatic primary production in a high-CO_2 world. Trends Ecol. Evol. 29, 223–232. https://doi.org/10.1016/j.tree.2014.02.006.

Menshutkin, V.V., Rukhovets, L.A., Filatov, N.N., 2014. Ecosystem modeling of freshwater lakes (review): 2. Models of freshwater lake's ecosystem. Water Res. 41, 32–45. https://doi.org/10.1134/S0097807814010084.

Morales-Pineda, M., Cózar, A., Laiz, I., et al., 2014. Daily, biweekly, and seasonal temporal scales of pCO_2 variability in two stratified Mediterranean reservoirs. J. Geophys. Res. Biogeosci. 119, 509–520. https://doi.org/10.1002/2013JG002317.

Nakayama, T., Pelletier, G.J., 2018. Impact of global major reservoirs on carbon cycle changes by using an advanced eco-hydrologic and biogeochemical coupling model. Ecol. Model. 387, 172–186. https://doi.org/10.1016/j.ecolmodel.2018.09.007.

Pacheco, F.S., Roland, F., Downing, J.A., 2014. Eutrophication reverses whole-lake carbon budgets. Inland Waters 4, 41–48. https://doi.org/10.5268/IW-4.1.614.

Pacheco, F.S., Soares, M.C.S., Assireu, A.T., et al., 2015. The effects of river inflow and retention time on the spatial heterogeneity of chlorophyll and water–air CO_2 fluxes in a tropical hydropower reservoir. Biogeosciences 12, 147–162. https://doi.org/10.5194/bg-12-147-2015.

Paranaíba, J.R., Barros, N., Mendonça, R., et al., 2018. Spatially resolved measurements of CO_2 and CH_4 concentration and gas-exchange velocity highly influence carbon-emission estimates of reservoirs. Environ. Sci. Technol. 52, 607–615. https://doi.org/10.1021/acs.est.7b05138.

Pei, H., Wang, Y., 2003. Eutrophication research of West Lake, Hangzhou, China: modeling under uncertainty. Water Res. 37, 416–428. https://doi.org/10.1016/S0043-1354(02)00287-7.

Reinfelder, J.R., 2010. Carbon concentrating mechanisms in eukaryotic marine phytoplankton. Annu. Rev. Mar. Sci. 3, 291–315. https://doi.org/10.1146/annurev-marine-120709-142720.

Roland, F., Vidal, L.O., Pacheco, F.S., et al., 2010. Variability of carbon dioxide flux from tropical (Cerrado) hydroelectric reservoirs. Aquat. Sci. 72, 283–293. https://doi.org/10.1007/s00027-010-0140-0.

Saidi, H., Koschorreck, M., 2017. CO_2 emissions from German drinking water reservoirs. Sci. Total Environ. 581-582, 10–18. https://doi.org/10.1016/j.scitotenv.2017.01.004.

Sandrini, G., Matthijs, H.C.P., Verspagen, J.M.H., et al., 2014. Genetic diversity of inorganic carbon uptake systems causes variation in CO_2 response of the cyanobacterium Microcystis. ISME J. 8, 589–600. https://doi.org/10.1038/ismej.2013.179.

Sandrini, G., Ji, X., Verspagen, J.M.H., et al., 2016. Rapid adaptation of harmful cyanobacteria to rising CO_2. Proc. Natl. Acad. Sci. 113, 9315–9320. https://doi.org/10.1073/pnas.1602435113.

Santoso, A.B., Hamilton, D.P., Hendy, C.H., et al., 2017. Carbon dioxide emissions and sediment organic carbon burials across a gradient of trophic state in eleven New Zealand lakes. Hydrobiologia 795, 341–354. https://doi.org/10.1007/s10750-017-3158-7.

Shapiro, J., 1997. The role of carbon dioxide in the initiation and maintenance of blue-green dominance in lakes. Freshw. Biol. 37, 307–323. https://doi.org/10.1046/j.1365-2427.1997.00164.x.

Shi, X., Li, S., Wei, L., et al., 2017. CO_2 alters community composition of freshwater phytoplankton: a microcosm experiment. Sci. Total Environ. 607, 69–77. https://doi.org/10.1016/j.scitotenv.2017.06.224.

Song, C., Gardner, K.H., Klein, S.J.W., et al., 2018. Cradle-to-grave greenhouse gas emissions from dams in the United States of America. Renew. Sust. Energ. Rev. 90, 945–956. https://doi.org/10.1016/j.rser.2018.04.014.

St. Louis, V.L., Kelly, C.A., Duchemin, É., et al., 2000. Reservoir surfaces as sources of greenhouse gases to the atmosphere: a global estimate. Bioscience 50, 766–775. https://doi.org/10.1641/0006-3568(2000)050[0766:RSASOG]2.0.CO;2.

Teodoru, C.R., Prairie, Y.T., Del Giorgio, P.A., 2011. Spatial heterogeneity of surface CO_2 fluxes in a newly created Eastmain-1 reservoir in northern Quebec, Canada. Ecosystems 14, 28–46. https://doi.org/10.1007/s10021-010-9393-7.

Tian, H., Ren, W., Yang, J., et al., 2015. Climate extremes dominating seasonal and interannual variations in carbon export from the Mississippi River Basin. Glob. Biogeochem. Cycles 29, 1333–1347. https://doi.org/10.1002/2014GB005068.

Tonetta, D., Staehr, P.A., Petrucio, M.M., 2017. Changes in CO_2 dynamics related to rainfall and water level variations in a subtropical lake. Hydrobiologia 794, 109–123. https://doi.org/10.1007/s10750-017-3085-7.

Tranvik, L.J., Downing, J.A., Cotner, J.B., et al., 2009. Lakes and reservoirs as regulators of carbon cycling and climate. Limnol. Oceanogr. 54, 2298–2314. https://doi.org/10.4319/lo.2009.54.6_part_2.2298.

Verspagen, J.M.H., Van de Waal, D.B., Finke, J.F., et al., 2014. Rising CO_2 levels will intensify phytoplankton blooms in eutrophic and hypertrophic lakes. PLoS One 9, e104325. https://doi.org/10.1371/journal.pone.0104325.

Vogt, R.J., St-Gelais, N.F., Bogard, M.J., et al., 2017. Surface water CO_2 concentration influences phytoplankton production but not community composition across boreal lakes. Ecol. Lett. 20, 1395–1404. https://doi.org/10.1111/ele.12835.

Wang, F., Wang, B., Liu, C.-Q., et al., 2011. Carbon dioxide emission from surface water in cascade reservoirs–river system on the Maotiao River, southwest of China. Atmos. Environ. 45, 3827–3834. https://doi.org/10.1016/j.atmosenv.2011.04.014.

Wang, X., He, Y., Yuan, X., et al., 2017. Greenhouse gases concentrations and fluxes from subtropical small reservoirs in relation with watershed urbanization. Atmos. Environ. 154, 225–235. https://doi.org/10.1016/j.atmosenv.2017.01.047.

Wang, W., Roulet, N.T., Kim, Y., et al., 2018. Modelling CO_2 emissions from water surface of a boreal hydroelectric reservoir. Sci. Total Environ. 612, 392–404. https://doi.org/10.1016/j.scitotenv.2017.08.203.

Wanninkhof, R., 1992. Relationship between wind speed and gas exchange over the ocean. J. Geophys. Res. Oceans 97, 7373–7382. https://doi.org/10.1029/92JC00188.

Wanninkhof, R., 2014. Relationship between wind speed and gas exchange over the ocean revisited. Limnol. Oceanogr. Methods 12, 351–362. https://doi.org/10.4319/lom.2014.12.351.

Weiss, R.F., 1974. Carbon dioxide in water and seawater: the solubility of a non-ideal gas. Mar. Chem. 2, 203–215. https://doi.org/10.1016/0304-4203(74)90015-2.

Wen, Z., Song, K., Shang, Y., et al., 2017. Carbon dioxide emissions from lakes and reservoirs of China: a regional estimate based on the calculated pCO_2. Atmos. Environ. 170, 71–81. https://doi.org/10.1016/j.atmosenv.2017.09.032.

Winder, M., Schindler, D.E., 2004. Climate change uncouples trophic interactions in an aquatic ecosystem. Ecology 85, 2100–2106. https://doi.org/10.1890/04-0151.

Wu, Z., Zeng, B., Li, R., et al., 2012. Combined effects of carbon and phosphorus levels on the invasive cyanobacterium, Cylindrospermopsis raciborskii. Phycologia 51, 144–150. https://doi.org/10.2216/10-87.1.

Xiao, S., Wang, Y., Liu, D., et al., 2013. Diel and seasonal variation of methane and carbon dioxide fluxes at Site Guojiaba, the Three Gorges Reservoir. J. Environ. Sci. 25, 2065–2071. https://doi.org/10.1016/S1001-0742(12)60269-1.

Yan, X., Xu, X., Wang, M., et al., 2017. Climate warming and cyanobacteria blooms: looks at their relationships from a new perspective. Water Res. 125, 449–457. https://doi.org/10.1016/j.watres.2017.09.008.